Published in final edited form as:
Magn Reson Med. 2009 June ; 61(6): 1310–1318. doi:10.1002/mrm.21877.

Spatial Distribution and Relationship of $T_{1\rho}$ and T_2 Relaxation Times in Knee Cartilage With Osteoarthritis

Xiaojuan Li[1,*], **Alex Pai**[2], **Gabrielle Blumenkrantz**[2], **Julio Carballido-Gamio**[1], **Thomas Link**[1], **Benjamin Ma**[3], **Michael Ries**[3], and **Sharmila Majumdar**[1]

[1] Musculoskeletal Quantitative Imaging Research (MQIR) Group, Department of Radiology, University of California, San Francisco, San Francisco, California, USA

[2] Department of Electrical Engineering and Computer Science, University of California, Berkeley, Berkeley, California, USA

[3] Department of Orthopaedic Surgery, University of California, San Francisco, San Francisco, California, USA

Abstract

$T_{1\rho}$ and T_2 relaxation time constants have been proposed to probe biochemical changes in osteoarthritic cartilage. This study aimed to evaluate the spatial correlation and distribution of $T_{1\rho}$ and T_2 values in osteoarthritic cartilage. Ten patients with osteoarthritis (OA) and 10 controls were studied at 3T. The spatial correlation of $T_{1\rho}$ and T_2 values was investigated using *Z*-scores. The spatial variation of $T_{1\rho}$ and T_2 values in patellar cartilage was studied in different cartilage layers. The distribution of these relaxation time constants was measured using texture analysis parameters based on gray-level co-occurrence matrices (GLCM). The mean *Z*-scores for $T_{1\rho}$ and T_2 values were significantly higher in OA patients vs. controls ($P < 0.05$). Regional correlation coefficients of $T_{1\rho}$ and T_2 *Z*-scores showed a large range in both controls and OA patients (0.2– 0.7). OA patients had significantly greater GLCM contrast and entropy of $T_{1\rho}$ values than controls ($P < 0.05$). In summary, $T_{1\rho}$ and T_2 values are not only increased but are also more heterogeneous in osteoarthritic cartilage. $T_{1\rho}$ and T_2 values show different spatial distributions and may provide complementary information regarding cartilage degeneration in OA.

Keywords

osteoarthritis; cartilage; magnetic resonance imaging; $T_{1\rho}$ (T_1rho); T_2.; texture analysis

Hyaline articular cartilage plays an important role in the function of diarthrodial joints. Degeneration of cartilage is also one of the most critical biomarkers in degenerative and traumatic joint diseases such as osteoarthritis (OA) (1). Current clinical evaluation of cartilage degeneration relies primarily on plain radiographs, which depict only gross osseous changes that tend to occur late in the disease. Cartilage loss can only be indirectly inferred by joint-space narrowing, and early changes in the articular cartilage may not be visible on plain radiographs.

Magnetic resonance imaging (MRI) of cartilage has improved greatly during the past decade (2). It offers multi-planar capabilities and high spatial resolution without ionizing radiation, and provides superior depiction of soft- tissue details. Cartilage morphology can be examined

*Correspondence to: Xiaojuan Li, Ph.D., Department of Radiology, University of California at San Francisco, 185 Berry Street, Suite 350, San Francisco, CA 94107. E-mail: xiaojuan.li@radiology.ucsf.edu.

qualitatively, and cartilage volume and thickness can be quantified using very high-resolution MR images. The most active development in this field, however, lies in imaging cartilage matrix biochemistry that is essential for detecting cartilage degeneration at the very early stages of the disease (3,4).

Hyaline cartilage consists of a small number of chondrocytes and a large extracellular matrix (ECM). The ECM is composed primarily of water and a mixture of amorphous and fibrous components. The amorphous component predominantly contains proteoglycans (PGs) that consist of highly negative-charged polysaccharide chains (glycos-aminoglycans [GAGs]). A key function of these aggregates is to provide a stable environment of high fixed-charge density (FCD), which is essential for imbibing and retaining water. The formed component of the ground substance is composed of collagen fibers (mainly type II) that interact electrostatically with the GAGs to form a cross-linked matrix. The distribution and orientation of collagen in cartilage demonstrates anatomical zones at microscopy. The collagen fibers are oriented parallel to the articular surface in the superficial zone, perpendicular in the radial zone, and arcade-like in the transitional zone. Early events during cartilage breakdown include the loss of PGs, changes in water content, and molecular-level changes in collagen (5). Early diagnosis of cartilage degeneration would require the ability to noninvasively detect changes in PG concentration and collagen integrity before gross morphologic changes occur.

Recent advances in imaging cartilage composition include $T_{1\rho}$ and T_2 relaxation time constant mapping. Immobilization of water protons in cartilage by the collagen-PG matrix promotes T_2 decay. Damage to the collagen-PG matrix and an increase of water contents in degenerating cartilage can increase T_2 values (6,7). The $T_{1\rho}$ parameter describes the spin-lattice relaxation in the rotating frame (8). It probes the slow-motion interactions between motion-restricted water molecules and their local macromolecular environment. Changes to the ECM, such as PG loss, may be reflected in the elevation of $T_{1\rho}$ (9,10).

Although previous studies have observed elevated $T_{1\rho}$ and T_2 values in OA patients, few studies have documented quantitative evaluation of the spatial distribution of $T_{1\rho}$ and T_2 values, and the correlation between these two parameters (11). Texture analysis can be used to examine the spatial distribution of pixel values and quantify the heterogeneity in an image (12). The most commonly used texture analysis parameters are those extracted from the gray-level co-occurrence matrix (GLCM) as proposed by Haralick et al. (13). The GLCM determines the frequency at which neighboring gray-level values occur in an image. Parameters derived from GLCM provide information on the variation between neighboring pixels and directly quantify the distribution of the image signal. Some very recent studies used this method to characterize the distribution of cartilage pixel values in anatomic images (14) and T_2 relaxation maps (15).

We previously observed significantly elevated mean cartilage $T_{1\rho}$ and T_2 values in patients with knee OA, and the increase was correlated with the severity of disease based on plain radiographs and morphologic MRI findings (16). The goals of this study, using the same patient cohort, were to 1) evaluate the spatial variation of $T_{1\rho}$ and T_2 relaxation time constants and the relationship of both techniques; and 2) investigate the spatial distribution of $T_{1\rho}$ and T_2 values using texture analysis.

MATERIALS AND METHODS

Subjects

Ten healthy volunteers (four female and six male, mean age = 41 years with a range from 28 to 74 years) and 10 patients with clinically diagnosed OA (three female and seven male, mean age = 56 years with a range from 37 to 72 years) were studied. All patients had clinical

symptoms and signs of OA (pain, stiffness or swelling of the joint) and demonstrated radiographic changes consistent with OA. The inclusion/exclusion criteria for the control subjects were no history of OA symptoms, no prior knee trauma, and no OA-related MR findings. The study was approved by the committee for human research at our institution, and all of the subjects gave informed consent.

Imaging Protocols

All MR exams were implemented on a 3T GE Excite Signa (GE Healthcare, Waukesha, WI) MR scanner using a quadrature transmit/receive knee coil (Clinical MR Solutions, Brookfield, WI). The protocol included six sequences: sagittal T_1-weighted spin-echo (SE) imaging (TR/TE = 700/13.5 ms, FOV = 16 cm, matrix = 288 × 224, bandwidth = 15.63 KHz, Number of excitations [NEX] = 2), sagittal and axial 3D water excitation high-resolution spoiled gradient-echo (SPGR) imaging (TR/TE = 15/6.7 ms, flip angle = 12, FOV = 16 cm, matrix = 512 × 512, slice thickness = 1 mm, bandwidth = 31.25 kHz, NEX = 0.75), fat-saturated T_2-weighted fast SE (FSE) images (TR/TE = 3700/68 ms, FOV = 14 cm, matrix = 288 × 224, slice thickness = 3 mm, echo train length [ETL] = 8, bandwidth = 16.5 kHz, NEX = 2), and axial $T_{1\rho}$-weighted and T_2-weighted images.

The multislice $T_{1\rho}$-weighted images were obtained using the sequence we previously developed based on spin-lock (SL) techniques and spiral image acquisition The technique was detailed in a previous publication (17) and was summarized as follows: The SL pulse cluster consisted of a hard 90° pulse followed by a SL pulse and a hard −90° pulse. The first 90° pulse applied along the *x*-axis flipped the longitudinal magnetization into the transverse plane along the *y*-axis. Then, a long low-power pulse was applied along the *y*-axis to spin-lock the magnetization. The second 90° pulse flipped this spin-locked magnetization back to the *z*-axis. The phase of the second half of the SL pulse was shifted 180° from the first half to reduce artifacts caused by B_1 inhomogeneity (18). Residual transverse magnetization was dephased by a crusher gradient. Magnetization stored along the *z*-axis was read out by a multislice spiral sequence. A spiral interleave from each prescribed slice was acquired in rapid succession. Any residual longitudinal magnetization was then spoiled using magnetization reset pulses consisting three sets of 90° excitations and spoiler gradients applied sequentially. This magnetization reset was followed by an operator-defined recovery time in order to ensure that the signal right before $T_{1\rho}$ preparation was the same independently of spin history. An RF cycling technique was used to eliminate T_1 contamination in the $T_{1\rho}$-weighted images. The duration of SL pulses, or the time of SL (TSL), determined the amount of $T_{1\rho}$ weighting in acquisition. The strength of SL was defined as the SL frequency (F_{SL}). The sequence was validated in phantoms and in vivo, and the average coefficient of variation was 0.86% in agarose phantoms and 4.8% in vivo, showing good reproducibility (17).

The acquisition parameters were: 14 interleaves/slice, 4096 points/interleaf, FOV = 16 cm, effective in-plane spatial resolution = 0.6 × 0.6 mm, slice thickness = 3 mm, skip = 1 mm, number of slices = 14 –16, TR/TE = 2000/5.8 ms, TSL = 20/40/60/80 ms, F_{SL} = 500 Hz, NEX = 1. The total acquisition time was approximately 13 minutes. The axial $T_{1\rho}$-weighted images were prescribed on sagittal SPGR images, covering regions from the top of the patellar cartilage to the femoral-tibial cartilage.

The T_2 quantification was also based on a magnetization preparation sequence with spiral imaging (19,20), To briefly summarize, the T_2 preparation pulses contained an MLEV train of nonselective composite $90_x180_y90_x$ refocusing pulses. The refocusing train was preceded and followed by a composite $90_x/90_{-x}$ ($360_x270_{-x}90_y/45_{-x}90_{-y}90_x45_y$) pulse pair for rotation of magnetization into and out of the transverse plane. Simulation suggested that this design of magnetization preparation, combining with effective correction for T_1 signal decay during each pulse, provided T_2 measurement accuracy within 5%, given B_1 offset within ±20% and B_0

offset ±2 ppm (21). All other prescription parameters of the T_2 sequence were identical to the $T_{1\rho}$ sequence except for TR/TE = 2000/6.7, 12, 28, 60 ms. The total acquisition time was approximately 11 min. The T_2 quantification was acquired subsequently and covered the same region as the $T_{1\rho}$ sequence.

Image Processing

$T_{1\rho}$ maps were reconstructed by fitting the image intensity pixel-by-pixel to the equation below using a Levenberg-Marquardt monoexponential fitting algorithm developed in-house:

$$S(TSL) \propto \exp(-TSL/T_{1\rho}) \quad [1]$$

$T_{1\rho}$-weighted images with the shortest TSL (and therefore with the highest SNR) were rigidly registered to high-resolution T_1-weighted SPGR images acquired in the same exam using the VTK CISG Registration Toolkit (22). Normalized Mutual Information (NMI) was used during registration (23). The 2D images were interpolated using a trilinear interpolation algorithm before the 3D volume registration. The transformation matrix was applied to the reconstructed $T_{1\rho}$ map.

Cartilage was segmented semiautomatically from the high-resolution SPGR images using an in-house-developed program with MATLAB based on edge detection and Bezier splines (24). Seven compartments were defined as shown in Fig. 1: posterior lateral femoral condyle (pLFC), posterior medial femoral condyle (pMFC), trochlea lateral femur (trLF), trochlea medial femur (trMF), lateral patellar (LP), central patellar (CP), and medial patellar (MP). The segmentation was corrected manually to avoid synovial fluid or other surrounding tissue. 3D cartilage contours were generated and overlaid on the registered $T_{1\rho}$ map.

Similarly, T_2 maps were reconstructed by fitting the image intensity pixel-by-pixel to the equation:

$$S(TE) \propto \exp(-TE/T_2) \quad [2]$$

T_2-weighted images with the shortest TE were rigidly registered to SPGR images, and the transformation matrix was applied to T_2 maps using the VTK CISG Registration Toolkit. The cartilage contours previously generated from SPGR images were also overlaid on the registered T_2 map.

To study the spatial variation of $T_{1\rho}$ and T_2 values along cartilage depth, the line profile of $T_{1\rho}$ and T_2 values from cartilage/bone interface to cartilage surface was generated in the patellar cartilage (Fig. 2). Eleven lines were generated, with four in LP, three in CP, and four in MP. The data were interpolated into 30 data points on each line. The data were then fitted to the function below as suggested by Smith et al. (25):

$$y=a+bx+cx^2+dx^3+e\exp(x) \quad [3]$$

where y is the $T_{1\rho}$ or T_2 values, and x is the cartilage depth normalized to 0 –1 (0: bone/cartilage interface; 1: cartilage surface). The mean $T_{1\rho}$ and T_2 data for each layer of cartilage were also calculated based on these line profile data with data point 1–15 for the deep or radial zone, data point 16 –25 for the transitional zone, and data point 26 –30 for the superficial zone.

To study the spatial correlation between $T_{1\rho}$ and T_2 values, $T_{1\rho}$ and T_2 Z-scores were calculated as:

$$Z_1=(\text{Volex}_1 - \text{Mean}_{\text{normal,compartment}})/\text{SD}_{\text{normal,compartment}} \quad [4]$$

where Voxel_1 is the $T_{1\rho}$ or T_2 in the voxel of interest, and $\text{Mean}_{\text{normal, comparment}}$ and $\text{SD}_{\text{normal, comparment}}$ are the mean and standard deviation of $T_{1\rho}$ or T_2 for all voxels of the normal knees in that compartment derived from healthy controls, respectively. The point-to-point correlation between the *Z*-scores of $T_{1\rho}$ and T_2 in each patient were calculated for each compartment and for the overall cartilage using a Pearson correlation.

Texture analysis was performed on a slice-by-slice basis on the cartilage $T_{1\rho}$ and T_2 maps in four subcompartments: MFC, LFC, trochlea (combing trLF and trMF), and patellar (combining LP, MP, and CP). The parameters were extracted from the GLCM. Analysis can be performed at a defined orientation (e.g., 0° and 90°) and a defined spacing (e.g., spacing = 1 for nearest-neighbor pixels). From GLCM, it is possible to calculate a set of at least 14 parameters. Three first-and second-degree texture parameters were calculated in this study:

$$\begin{aligned} Contrast &= \sum_{n=0}^{N-1} n^2 \left[\sum_{|i-j|=n} \left(\frac{P(i,j)}{R} \right) \right] \\ ASM &= \sum_{i=1}^{N} \sum_{j=1}^{N} \left(\frac{P(i,j)}{R} \right)^2 \\ Entropy &= \sum_{i=1}^{N} \sum_{j=1}^{N} P(i,j)(-\ln P(i,j)) \end{aligned} \quad [5]$$

where *P* represents the probability of the co-occurrence of pixel values *i* and *j* in an image. *N* represents the number of distinct gray levels in the quantized image. *R* is a normalizing constant. The contrast feature is a measure of the contrast of the amount of local variation present in an image. Angular second moment (ASM) is a measure of order in an image, while entropy is a measure of disorder in an image. These parameters were chosen because we wanted to include parameters from the different groups of texture measures. These groups are the contrast group (which contains the contrast parameter) and the orderliness group (which contains entropy and ASM).

Texture parameters of $T_{1\rho}$ and T_2 maps were calculated at 0° (corresponding to the anterior–posterior axis) and at 90° (corresponding to the superior–inferior axis), with pixel offsets ranging from 1 to 3 pixels. The pixel offset range was chosen based on the fact that approximately 3– 4 pixels span the cartilage thickness.

Statistical Analysis

Student's *t*-test was used to compare the mean $T_{1\rho}$ and T_2 *Z*-scores between control subjects and OA patients in each subcompartment. The Pearson correlation coefficients of $T_{1\rho}$ and T_2 *Z*-scores were calculated in each subcompartment. Student's *t*-test was also used to compare the texture parameters between controls and OA patients.

RESULTS

$T_{1\rho}$ and T_2 *Z*-scores in Controls and OA Patients

The average *Z*-score for $T_{1\rho}$ and T_2 values was significantly higher in patients with OA than control subjects (2.14 ± 0.98 in OA vs. 0.004 ± 0.69 in controls, $P > 0.0003$ for $T_{1\rho}$ *Z*-scores, and 2.08 ± 1.44 vs. −0.26 ± 0.50, $P > 0.002$ for T_2 *Z*-scores, Table 1). Figure 3 shows representative images of $T_{1\rho}$ and T_2 maps for a healthy control subject and a patient with OA.

In the femoral subcompartments, the $T_{1\rho}$ and T_2 *Z*-scores were also significantly higher in OA patients than those in controls. The difference was not significant, however, in the patellar subcompartments, except for the $T_{1\rho}$ *Z*-score in the central patella compartment.

No significant difference was found in the correlation between $T_{1\rho}$ and T_2 *Z*-scores of overall cartilage between controls and OA patients (0.522 ± 0.183, ranging from 0.221 to 0.763 in OA patients vs. 0.624 ± 0.060, ranging from 0.547 to 0.726 in controls, $P > 0.173$). In the subcompartments, the correlation coefficients of $T_{1\rho}$ and T_2 *Z*-scores were higher in the medial compartments (pMFC and trMF) and lower in the patellar compartments (Fig. 4). This difference was significant in trMF ($P < 0.05$). Figure 3 shows an example of a patient, where $T_{1\rho}$ and T_2 *Z*-scores had a low correlation coefficient of 0.289 in overall cartilage. The correlation coefficients of $T_{1\rho}$ and T_2 *Z*-scores in the patient in Fig. 3 were 0.435, 0.598, 0.225, 0.605, 0.477, 0.734, 0.294, and 0.289 for pLFC, pMFC, trLF, trMF, LP, MP, and CP, respectively.

$T_{1\rho}$ and T_2 Spatial Variation in Patellar Cartilage

$T_{1\rho}$ and T_2 values increased significantly from the deep layer to the superficial layer of the patella. The difference in $T_{1\rho}$ and T_2 values between each layer were significant ($P < 0.05$). Figure 5 shows the line profile of $T_{1\rho}$ and T_2 values from bone cartilage interface to the cartilage surface for both controls and patients. When the data were compared between controls and OA patients within the subregions and sublayers of the patella, only $T_{1\rho}$ values in the superficial layer of MP and in all the layers in CP, and T_2 values in the deep layer of the MP, were significantly higher in OA patients than those in controls. No significant differences were observed on the lateral side, as shown in Table 2.

Texture Analysis

OA patients had greater overall contrast and entropy, but lower overall GLCM ASM of cartilage $T_{1\rho}$ and T_2 than controls at 0° and 90° in all pixel offsets. These differences were significant ($P < 0.05$) in the GLCM contrast (0°, 1– 4 pixel offset and 90°, 1– 4 pixel offset), and entropy (0°, 1 pixel offset and 90°, 1 pixel offset) of cartilage $T_{1\rho}$, while no significant difference was found in cartilage T_2. Figure 6 shows the GLCM contrast, entropy, and ASM of $T_{1\rho}$ and T_2 in 0° and 1 pixel offset as an example.

The texture measurements in all the compartments, except for the entropy and ASM of the patella $T_{1\rho}$ and T_2, coincided with the overall trends. Contrast was significantly different between control and OA patients in the medial femur T_2 ($P < 0.05$). ASM was significantly different between control and OA patients in the trochlea $T_{1\rho}$ ($P < 0.05$).

The ASM was the lowest and entropy was the highest in MFC compartments for both $T_{1\rho}$ and T_2 values. The difference was significant in patients ($P < 0.008$, the significance level was adjusted for multicomparison) but not in controls. As an example, Fig. 7 shows the $T_{1\rho}$ ASM and entropy at 90° and 1 pixel offset in each compartment in controls and in OA patients.

DISCUSSION

In this study the spatial correlation and distribution of in vivo $T_{1\rho}$ and T_2 relaxation time constants in osteoarthritic and normal cartilage were investigated. Previously, Regatte et al. (11) compared average $T_{1\rho}$ and T_2 values in bovine (26) and human cartilage specimens. To our best knowledge, this study is the first documentation correlating pixel-by-pixel in vivo $T_{1\rho}$ and T_2 values in controls and OA subjects, and quantifying the spatial distribution of these relaxation time constants using texture analysis based on co-occurrence matrices.

Cartilage $T_{1\rho}$ and T_2 *Z*-scores were significantly higher in patients with knee OA than in healthy control subjects, which is consistent with previous observations of elevated $T_{1\rho}$ (16,27) and T_2 values in degenerated cartilage (6,7,16). This result suggests that $T_{1\rho}$ and T_2 may be valuable diagnostic tools in evaluating early stages of cartilage degeneration by detecting biochemical changes in the cartilage matrix.

Previous studies showed that collagen structure and orientation are dominating factors that affect T_2 relaxation in cartilage. This results in the "magic angle" effect and the commonly seen laminar appearance in cartilage imaging (28,29). During cartilage degeneration, T_2 has been found to correlate poorly with PG content in controlled in vitro studies (26,30). In $T_{1\rho}$ quantification experiments, the SL techniques reduce dipolar interactions and therefore reduce the dependence of the relaxation time constant on collagen fiber orientation (31). This may enable more accurate diagnoses of early degenerative changes in cartilage. $T_{1\rho}$ relaxation rate ($1/T_{1\rho}$) has been shown to decrease linearly with decreasing PG content in ex vivo bovine patellae (9) and has been proposed as a more specific indicator of PG content than T_2 relaxation in trypsinized cartilage (26).

The mechanism of $T_{1\rho}$ relaxation time in biological tissues, particularly in cartilage, is not fully understood yet. Using native and immobilized protein solution, Makela et al. (32) suggested that proton exchange between the protein side-chain groups and bulk water contribute significantly to the $T_{1\rho}$ relaxation. Based on spectroscopy experiments with peptide solutions, GAG solutions and bovine cartilage samples before and after PG degradation, Duvvuri et al. (33) further suggested that in cartilage hydrogen exchange from NH and OH groups to water may dominate the low frequency (0 –1.5 KHz) water $T_{1\rho}$ dispersion. They speculated that increase of the low-frequency correlation rate with PG loss could be the result of increased proton exchange rates. Other evidence of a proton exchange pathway is the PH dependency of $T_{1\rho}$ values in the ischemic rat brain tissues (34). Mlynarik et al. (35), on the other hand, have suggested that the dominant relaxation mechanism in the rotating frame in cartilage at $B_0 \leq 3$T seems to be dipolar interaction. The contribution of scalar relaxation caused by proton exchange is only relevant at high fields, such as 7T. Clearly, further investigations are needed to better understand this relaxation mechanism.

Although further work is needed to elucidate the different mechanisms that contribute to $T_{1\rho}$ and T_2 relaxations, we hypothesize that these two parameters may provide complementary information regarding macromolecular changes in cartilage. In order to study the relationship between the spatial distribution of these two parameters, $T_{1\rho}$ and T_2 values were normalized with the concept of the *Z*-score. The *Z*-score conversion normalizes the $T_{1\rho}$ and T_2 values for each subject with the mean value of the control subjects in each defined compartment. This method allows the differences between cartilage compartments, if present, to be removed and compared on a common standard, and the $T_{1\rho}$ and T_2 images may be correlated pixel-by-pixel in any given region. A high correlation coefficient implies a high degree of agreement between these relaxation time constants, while a low one suggests discrepancy between these two parameters.

In this study, $T_{1\rho}$ and T_2 *Z*-scores showed a large range of correlations in both controls and patients. In OA patients, the correlation coefficients range from 0.2 to 0.7. In vivo $T_{1\rho}$ and T_2 mapping may be valuable for assessing regional heterogeneity in cartilage degeneration in OA. When we examined each subcompartment separately, trMF and pMFC showed higher *Z*-score correlation coefficients in patients than in controls, while the correlation coefficients were lower in patellar subcompartments in patients than in controls. In OA, the femoral-tibial joint normally has more advanced degeneration than the patellar-femoral joint. We hypothesize that at early stages of degeneration, $T_{1\rho}$ may be more sensitive to PG loss, while T_2 may be more sensitive to collagen network modification. Thus, a decreased correlation may be

observed, as shown in patellar compartments. However, at relatively late stages of degeneration, $T_{1\rho}$ and T_2 values are both affected by severe PG loss, collagen destruction, and hydration changes, and therefore $T_{1\rho}$ and T_2 values can be correlated to each other.

We further examined the spatial variation of $T_{1\rho}$ and T_2 values in patellar cartilage. Patellar cartilage was selected because it contains the thickest cartilage in the knee and on average includes four pixels crossing the cartilage in both controls and patients. After interpolation, the cartilage was divided into deep, transitional, and superficial zones, and lateral, medial, and central regions, resulting in a total of nine subregions. The line profiles of $T_{1\rho}$ and T_2 values show that these relaxation time constants increase from the bone/cartilage interface to the cartilage surface.

This relatively monotonic increasing trend of T_2 values and the range of T_2 values (from 20 to 60 ms) are consistent with prior work at 3T (6,36). In a more recent work, however, investigators observed high T_2 values at the bone/cartilage interface (74.1 ± 5.4 ms) (25). It decreased at a normalized distance of 0.33, and then increased monotonically to the articular surface. The authors attributed the high T_2 values in the deep zone to the potential partial voluming and chemical shift misregistration artifact at the bone/cartilage interface. In this study, a spectral-spatial RF pulse was used to suppress the fat signal. Therefore, the chemical shift misregistration artifact was minimized.

The spatial variation of the $T_{1\rho}$ values was consistent with previous observations in bovine cartilage (10) and human cartilage specimens (11). To our knowledge, no in vivo $T_{1\rho}$ line profiles in human cartilage have been reported. Although the trends of $T_{1\rho}$ and T_2 values are similar, $T_{1\rho}$ shows a larger dynamic range from the bone/cartilage interface to the cartilage surface, and a larger difference between controls and patients, particularly in the superficial layer, as shown in Fig. 5. When the data were further compared between controls and OA patients within the subregions and sublayers in patellar cartilage, $T_{1\rho}$ showed significant differences in the central regions of all layers. The $T_{1\rho}$ values were also significantly higher in the superficial layers on the medial side, but not in the transitional or deep layers. No significant differences were observed in T_2 values, except for the deep layer on medial side. These results suggest that 1) in patellar cartilage, the degeneration in cartilage may start from the central regions; and 2) $T_{1\rho}$ is more sensitive for detecting early degeneration than T_2 values.

As spatial variation was observed in this study and a number of previous studies, texture analysis provides a means to quantify their distribution. In this study, overall elevated contrast and entropy measurements, and lower ASM measurements of both $T_{1\rho}$ and T_2 values were observed in patients with OA when compared to controls. These differences, however, again appear more prevalent in $T_{1\rho}$ measurements, as shown in Fig. 6. The results indicate that these relaxation time constants are not only increased but are also more heterogeneous in osteoarthritic cartilage.

This observation of increasing T_2 heterogeneity in degenerated cartilage is consistent with results from Blumenkrantz et al. (15). They demonstrated that mild OA patients ($N = 8$) had significantly higher GLCM entropy and lower ASM of cartilage T_2 values than controls ($N = 14$). To our knowledge, no previous studies have documented in vivo $T_{1\rho}$ spatial heterogeneity in OA cartilage quantitatively. Our results suggest that the texture analysis provides information on spatial heterogeneity of $T_{1\rho}$ and T_2 values, and may be a valuable tool for detecting cartilage degeneration in OA.

For ASM and entropy measurements of $T_{1\rho}$ and T_2, the findings in the patellar cartilage behaved in an opposite manner of the overall trend. ASM of the patellar cartilage was significantly different between control and OA patients in $T_{1\rho}$ and T_2 at 0° and 90° at all pixel offsets. In OA, the cartilage degeneration occurs more often and more profoundly in weight-bearing areas

of the femoral-tibial joints. The unique behavior of patellar cartilage could be related to its reduced load-bearing requirements during stance and level walking compared to the tibiofemoral compartments, and therefore develops different degeneration behavior or may be at a different stage of degeneration compared to the tibiofemoral joints.

There are several limitations of this study. Both $T_{1\rho}$- and T_2-weighted images were acquired in an axial orientation. The spiral acquisition does not allow the use of an anti-aliasing filter, which is necessary for sagittal or coronal plane acquisition with a knee coil. Thus, only the anterior (trochlea) and posterior femoral condyle regions in the tibiofemoral joint are available. The tibia and the central portion of the femoral condyle could not be adequately analyzed. Further, the acquisition was in a 2D mode with 1-mm gap between slices. 3D information can be obtained only after interpolation between slices. $T_{1\rho}$- and T_2- weighted images with 3D acquisition may help to reduce slice thickness and obtain the true 3D information (27,37). Due to the limited image resolution (0.5 mm in-plane), only the patellar cartilage was analyzed for the spatial variation of relaxation time constants along different depths of cartilage. Other limitations include that the $T_{1\rho}$ and T_2 quantification was based on monoexponential decay. Errors may be introduced due to contribution from short relaxation time constant components (38).

In conclusion, $T_{1\rho}$ and T_2 quantification are valuable diagnostic tools for early detection of OA. These relaxation time constants are not only increased but are also more heterogeneous in osteoarthritic cartilage. $T_{1\rho}$ and T_2 show different spatial distributions and may provide complementary information regarding cartilage degeneration in OA. Combining these two parameters may further improve our capability to diagnose early cartilage degeneration and injury.

Acknowledgments

National Institutes of Health; Grant numbers: K25 AR053633; R01 AR46905.

We thank Eric Han from the Applied Science Laboratory, GE Healthcare, for his help with sequence development, and Anjali Prasad for editing the manuscript.

References

1. Brandt, KD.; Doherty, M.; Lohmander, LS., editors. Osteoarthritis. New York: Oxford University Press; 1998.
2. Link T, Stahl R, Woertler K. Cartilage imaging: motivation, techniques, current and future significance. Eur Radiol 2007;17:1135–1146. [PubMed: 17093967]
3. Gray M, Burstein D, Xia Y. Biochemical (and functional) imaging of articular cartilage. Seminars in musculoskeletal radiology 2001;5:329–343. [PubMed: 11745049]
4. Borthakur A, Mellon E, Niyogi S, Witschey W, Kneeland J, Reddy R. Sodium and T1rho MRI for molecular and diagnostic imaging of articular cartilage. NMR Biomed 2006;19:781–821. [PubMed: 17075961]
5. Dijkgraaf LC, de Bont LG, Boering G, Liem RS. The structure, biochemistry, and metabolism of osteoarthritic cartilage: a review of the literature. J Oral Maxillofac Surg 1995;53:1182–1192. [PubMed: 7562173]
6. Mosher TJ, Dardzinski BJ, Smith MB. Human articular cartilage: influence of aging and early symptomatic degeneration on the spatial variation of T2—preliminary findings at 3 T. Radiology 2000;214:259–266. [PubMed: 10644134]
7. Dunn TC, Lu Y, Jin H, Ries MD, Majumdar S. T2 relaxation time of cartilage at MR imaging: comparison with severity of knee osteoarthritis. Radiology 2004;232:592–598. [PubMed: 15215540]
8. Redfield AG. Nuclear spin thermodynamics in the rotating frame. Science 1969;164:1015–1023. [PubMed: 17796604]

9. Duvvuri U, Reddy R, Patel SD, Kaufman JH, Kneeland JB, Leigh JS. T1rho-relaxation in articular cartilage: effects of enzymatic degradation. Magn Reson Med 1997;38:863–867. [PubMed: 9402184]
10. Akella SV, Regatte RR, Gougoutas AJ, Borthakur A, Shapiro EM, Kneeland JB, Leigh JS, Reddy R. Proteoglycan-induced changes in T1rho-relaxation of articular cartilage at 4T. Magn Reson Med 2001;46:419–423. [PubMed: 11550230]
11. Regatte R, Akella S, Lonner J, Kneeland J, Reddy R. T1rho relaxation mapping in human osteoarthritis (OA) cartilage: comparison of T1rho with T2. J Magn Reson Imaging 2006;23:547–553. [PubMed: 16523468]
12. Petrou, M.; Sevilla, PG. Dealing with texture. Chichester, UK: John Wiley & Sons; 2006.
13. Haralick R, Shanmugam K, Dinstein I. Textural features for image classification. IEEE Trans Syst Man Cybernet 1973;3:610–618.
14. Qazi A, Folkesson J, Pettersen P, Karsdal M, Christiansen C, Dam E. Separation of healthy and early osteoarthritis by automatic quantification of cartilage homogeneity. Osteoarthritis Cartilage 2007;15:1199–1206. [PubMed: 17493841]
15. Blumenkrantz, G.; Stahl, R.; Carballido-Gamio, J.; Link, T.; Majumdar, S. Entropy of cartilage T2 maps in patients with osteoarthritis. Proceedings of the 11th World Congress on Osteoarthritis, Prague, Czech Republic; 2006.
16. Li X, Ma C, Link T, Castillo D, Blumenkrantz G, Lozano J, Carballido-Gamio J, Ries M, Majumdar S. In vivo T1rho and T2 mapping of articular cartilage in osteoarthritis of the knee using 3 Tesla MRI. Osteoarthritis Cartilage 2007;15:789–797. [PubMed: 17307365]
17. Li X, Han E, Ma C, Link T, Newitt D, Majumdar S. In vivo 3T spiral imaging based multi-slice T (1rho) mapping of knee cartilage in osteoarthritis. Magn Reson Med 2005;54:929–936. [PubMed: 16155867]
18. Charagundla SR, Borthakur A, Leigh JS, Reddy R. Artifacts in T(1rho)-weighted imaging: correction with a self-compensating spin-locking pulse. J Magn Reson 2003;162:113–121. [PubMed: 12762988]
19. Brittain JH, Hu BS, Wright GA, Meyer CH, Macovski A, Nishimura DG. Coronary angiography with magnetization-prepared T2 contrast. Magn Reson Med 1995;33:689–696. [PubMed: 7596274]
20. Foltz W, Al-Kwifi O, Sussman M, Stainsby J, GAW. Optimized spiral imaging for measurement of myocardial T2 relaxation. Magn Reson Med 2003;49:1089–1097. [PubMed: 12768587]
21. Foltz W, Stainsby J, Wright G. T2 accuracy on a whole-body imager. Magn Reson Med 1997;38:759–768. [PubMed: 9358450]
22. Rueckert D, Sonoda LI, Hayes C, Hill DL, Leach MO, Hawkes DJ. Nonrigid registration using free-form deformations: application to breast MR images. IEEE Trans Med Imaging 1999;18:712–721. [PubMed: 10534053]
23. Pluim J, Maintz J, Viergever M. Mutual-information-based registration of medical images: a survey. IEEE Trans Med Imaging 2003;22:986–1004. [PubMed: 12906253]
24. Carballido-Gamio J, Bauer JSRS, Lee KY, Krause S, Link TM, Majumdar S. Inter-subject comparison of MRI knee cartilage thickness. Med Image Anal 2008;12(2):120–135. [PubMed: 17923429]
25. Smith HE, Mosher TJ, Dardzinski BJ, Collins BG, Collins CM, Yang QX, Schmithorst VJ, Smith MB. Spatial variation in cartilage T2 of the knee. J Magn Reson Imaging 2001;14:50–55. [PubMed: 11436214]
26. Regatte RR, Akella SV, Borthakur A, Kneeland JB, Reddy R. Proteoglycan depletion-induced changes in transverse relaxation maps of cartilage: comparison of T2 and T1rho. Acad Radiol 2002;9:1388–1394. [PubMed: 12553350]
27. Regatte RR, Akella SV, Wheaton AJ, Lech G, Borthakur A, Kneeland JB, Reddy R. 3D-T1rho-relaxation mapping of articular cartilage: in vivo assessment of early degenerative changes in symptomatic osteoarthritic subjects. Acad Radiol 2004;11:741–749. [PubMed: 15217591]
28. Xia Y, Farquhar T, Burton-Wuster N, Ray E, Jelinski L. Diffusion and relaxation mapping of cartilage-bone plugs and excised disks using microscopic magnetic resonance imaging. Magn Reson Med 1994;31:273–282. [PubMed: 8057798]
29. David-Vaudey E, Ghosh S, Ries M, Majumdar S. T2 relaxation time measurements in osteoarthritis. Magn Reson Imaging 2004;22:673–682. [PubMed: 15172061]

30. Nieminen MT, Toyras J, Rieppo J, Hakumaki JM, Silvennoinen J, Helminen HJ, Jurvelin JS. Quantitative MR microscopy of enzymatically degraded articular cartilage. Magn Reson Med 2000;43:676–681. [PubMed: 10800032]

31. Akella SV, Regatte RR, Wheaton AJ, Borthakur A, Reddy R. Reduction of residual dipolar interaction in cartilage by spin-lock technique. Magn Reson Med 2004;52:1103–1109. [PubMed: 15508163]

32. Makela HI, Grohn OH, Kettunen MI, Kauppinen RA. Proton exchange as a relaxation mechanism for T1 in the rotating frame in native and immobilized protein solutions. Biochem Biophys Res Commun 2001;289:813–818. [PubMed: 11735118]

33. Duvvuri U, Goldberg AD, Kranz JK, Hoang L, Reddy R, Wehrli FW, Wand AJ, Englander SW, Leigh JS. Water magnetic relaxation dispersion in biological systems: the contribution of proton exchange and implications for the noninvasive detection of cartilage degradation. Proc Natl Acad Sci USA 2001;98:12479–12484. [PubMed: 11606754]

34. Kettunen M, Gröhn O, Silvennoinen M, Penttonen M, Kauppinen R. Effects of intracellular pH, blood, and tissue oxygen tension on T1rho relaxation in rat brain. Magn Reson Med 2002;48:470–477. [PubMed: 12210911]

35. Mlynarik V, Szomolanyi P, Toffanin R, Vittur F, Trattnig S. Transverse relaxation mechanisms in articular cartilage. J Magn Reson 2004;169:300–307. [PubMed: 15261626]

36. Dardzinski BJ, Mosher TJ, Li S, Van Slyke MA, Smith MB. Spatial variation of T2 in human articular cartilage. Radiology 1997;205:546–550. [PubMed: 9356643]

37. Li X, Han E, Busse R, Majumdar S. In vivo T1rho mapping in cartilage using 3D magnetization-prepared angle-modulated partitioned k-space spoiled gradient echo snapshots (3D MAPSS). Magn Reson Med 2008;59:298–307. [PubMed: 18228578]

38. Shinar H, Navon G. Multinuclear NMR and microscopic MRI studies of the articular cartilage nanostructure. NMR Biomed 2006;19:877–893. [PubMed: 17075957]

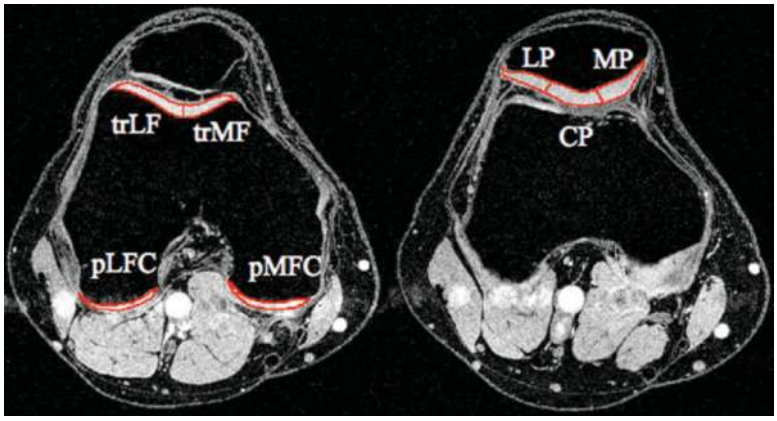

FIG. 1.

Definition of subcompartments of cartilage. trLF: lateral side of trochlea; trMF: medial side of trochlea; LFC: lateral femoral condyle; MFC: medial femoral condyle; LP: lateral side of patella; CP: central part of patella; MP: medial side of patella.

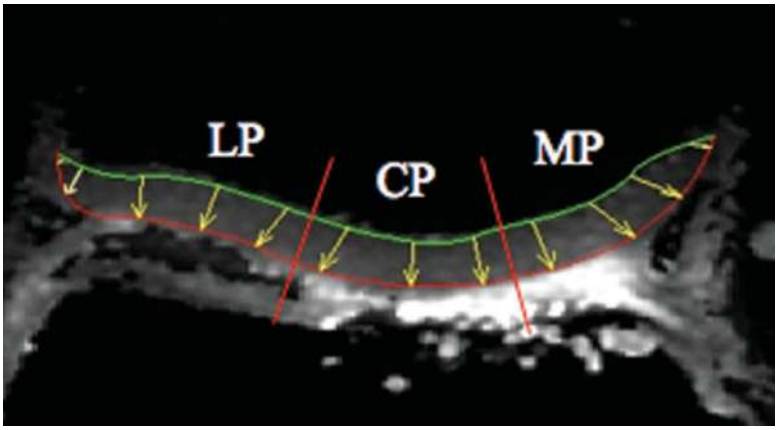

FIG. 2.

Line profile definition from bone/cartilage interface to cartilage surface in patellar cartilage. There are four lines defined in LP, three in CP, and four in MP, resulting in a total of 11 lines. There are 30 data points on each line after interpolation.

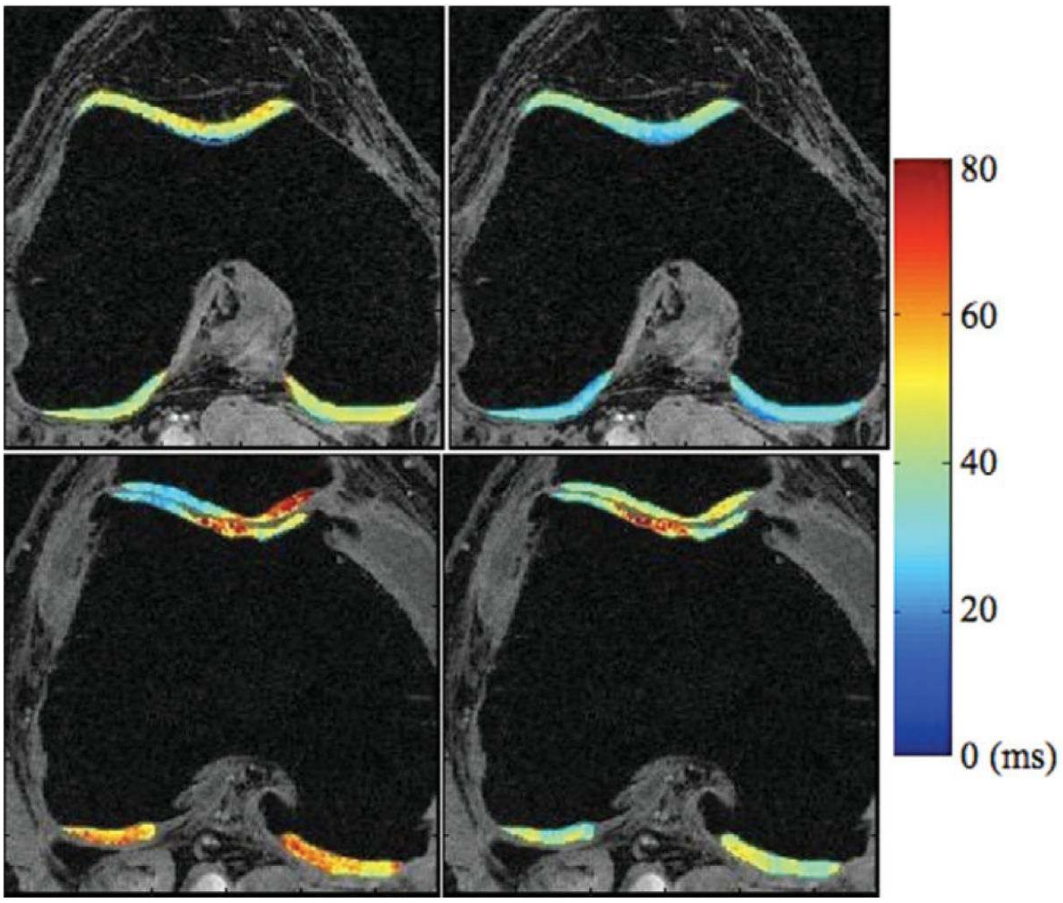

FIG. 3.

$T_{1\rho}$ (left) and T_2 (right) maps of a healthy control (upper row) and an OA subject (lower row). Significantly elevated $T_{1\rho}$ and T_2 values were observed in the patient. $T_{1\rho}$ and T_2 showed different spatial elevations in the patient.

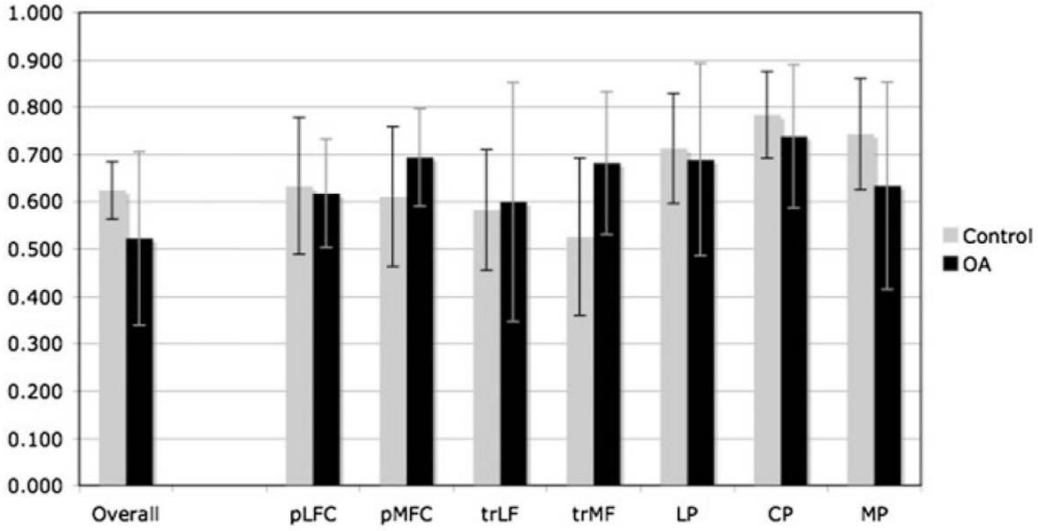

FIG. 4.

Correlation coefficients of $T_{1\rho}$ and T_2 *Z*-scores in overall cartilage and in each subcompartment. The overall correlation co-efficient decreased in patients, but not significantly ($P > 0.05$). The correlation coefficient increased in pMFC and trMF ($P < 0.05$ in trMF) and decreased in patellar subcompartments.

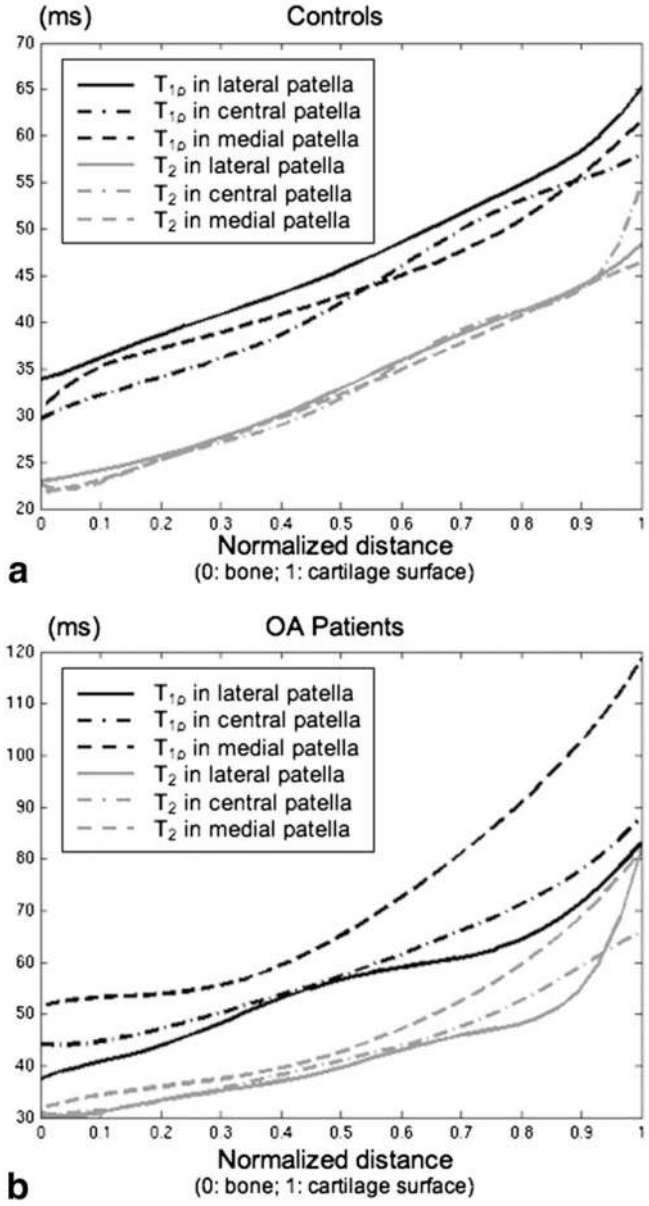

FIG. 5.

$T_{1\rho}$ and T_2 line profiles in patellar cartilage in controls (**a**) and OA patients (**b**). Both $T_{1\rho}$ and T_2 values increased significantly from the bone/cartilage interface to the cartilage surface.

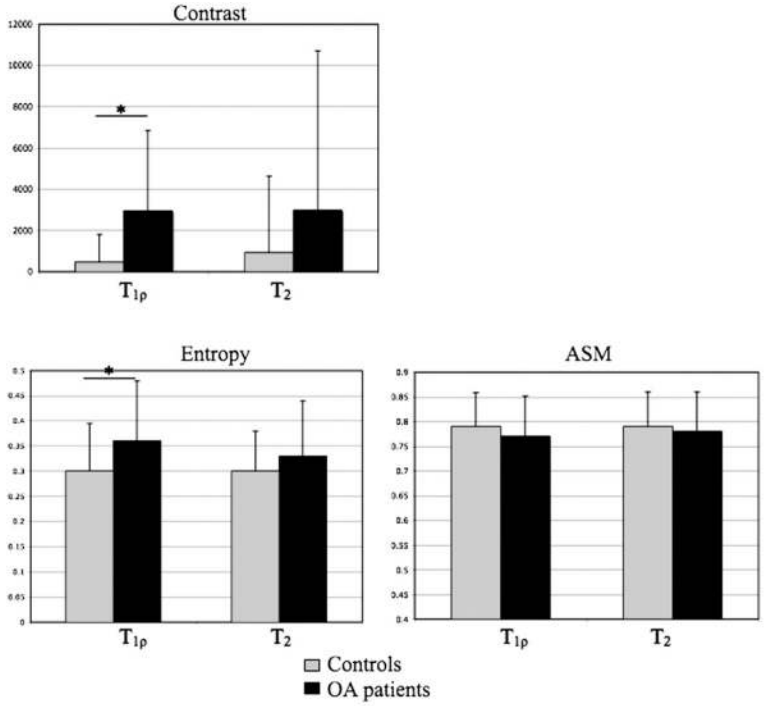

FIG. 6.

Texture parameters of $T_{1\rho}$ and T_2 values in overall cartilage in controls and OA patients in 0° and 1 pixel offset. OA subjects had greater overall contrast and entropy, but lower overall ASM of cartilage $T_{1\rho}$ and T_2 than controls at 0° and 90° in all pixel offsets. These differences were significant ($P < 0.05$) in the GLCM contrast, and entropy of cartilage $T_{1\rho}$ as indicated by * in the figure, while no significant difference was found in cartilage T_2.

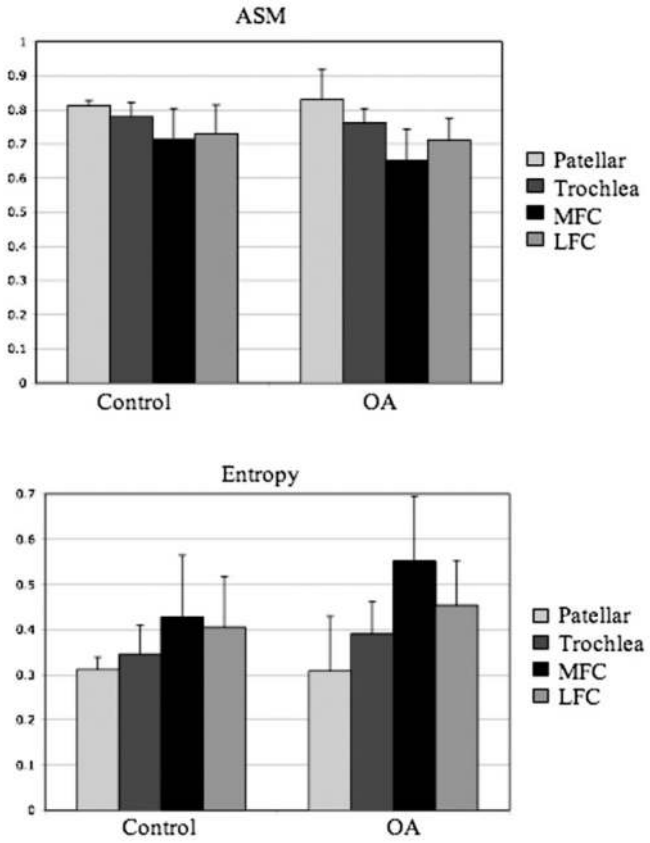

FIG. 7.

$T_{1\rho}$ ASM and entropy at 90° and 1 pixel offset in each compartment in controls and OA patients. The ASM was the lowest and the entropy was the highest in MFC compartments for both $T_{1\rho}$ and T_2 values. The difference was significant in patients ($P < 0.008$, the significance level was adjusted for multicomparison) but not in controls. T_2 ASM and entropy parameters showed similar patterns (data not shown).

Table 1

$T_{1\rho}$ and T_2 Z-Scores in Each Subcompartment in Controls and OA Patients*

a. $T_{1\rho}$ Z-Scores in Each Subcompartment

		pLFC	pMFC	trLF	trMF	PL	PR	PM	Overall
Controls	Mean	0.09	−0.12	0.02	0.15	0.06	0.19	0.14	0.004
	SD	1.03	1.00	1.07	0.95	1.07	0.87	0.97	0.69
OA	Mean	2.21	3.35	2.33	2.21	1.85	5.68	6.08	2.14
	SD	2.20	1.67	1.10	1.43	2.37	4.49	10.54	0.98
P values		**0.047**	**0.001**	**0.001**	**0.009**	0.084	**0.013**	0.170	**0.0003**

b. T_2 Z-Scores in Each Subcompartment

		pLFC	pMFC	trLF	trMF	PL	PR	PM	Overall
Controls	Mean	0.15	−0.05	0.01	0.09	0.18	0.21	0.17	−0.26
	SD	0.96	1.05	1.07	1.03	0.89	0.83	0.92	0.50
OA	Mean	3.58	5.28	2.59	2.95	1.03	2.39	1.81	2.08
	SD	2.19	2.56	1.65	1.74	1.79	2.81	2.25	1.44
P values		**0.005**	**0.001**	**0.005**	**0.004**	0.141	0.051	0.063	**0.002**

* Significant *P* values are in bold.

Table 2

$T_{1\rho}$ and T_2 Values in Subregions of Patellar Cartilage in Controls and OA Patients*

a. $T_{1\rho}$ Values in Patellar Subcompartments

		Lateral			**Central**			**Medial**		
		Deep	**Trans**	**Sup**	**Deep**	**Trans**	**Sup**	**Deep**	**Trans**	**Sup**
Controls	Mean	38.2	46.9	56.9	35.2	48.1	55.8	38.9	50.0	59.6
	SD	8.7	9.9	14.7	6.4	4.0	7.4	6.3	7.9	12.0
OA	Mean	41.9	54.7	67.0	45.2	58.8	73.5	51.6	72.4	99.1
	SD	15.0	13.2	17.1	10.6	13.1	17.1	22.1	36.3	50.2
P-values		0.53	0.17	0.19	**0.03**	**0.04**	**0.02**	0.13	0.10	0.05

b. T_2 Values in Patellar Subcompartments

		Lateral			Central			Medial		
		Deep	Trans	Sup	Deep	Trans	Sup	Deep	Trans	Sup
Controls	Mean	31.3	37.9	49.5	28.8	39.8	50.1	30.3	42.2	54.6
	SD	37.5	40.7	57.1	32.3	43.1	54.9	34.7	47.3	66.3
OA	Mean	3.8	4.5	7.5	4.2	3.2	8.1	5.1	5.4	11.9
	SD	13.5	12.3	31.3	8.0	10.0	14.5	8.5	15.8	29.4
P-values		0.06	0.30	0.26	0.08	0.14	0.16	**0.04**	0.16	0.09

Deep = deep or radial zone, Trans = transitional zone, Sup = superficial zone.

*Significant *P* values are in bold.